International Journal of
Automotive Manufacturing and Materials (IJAMM)

Scilight

Article

Check for updates

Study on Ion Current Characteristics and Reaction Mechanism of Oxygen-Enriched Ammonia Combustion

Jie Xu, Guangyu Dong *, Yanxiong Zhou, Xian Li, and Liguang Li

School of Automotive and Energy Engineering, Tongji University, Shanghai 201804, China
* Correspondence: g.dong@tongji.edu.cn
Received: 5 March 2026; Revised: 24 March 2026; Accepted: 13 April 2026; Published: 28 April 2026

Abstract: To develop a diagnosis of ammonia-hydrogen blended combustion based on ion current detection technology, this study investigates the pressure and ion current waveform characteristics of oxygen-enriched ammonia-hydrogen combustion using a constant volume combustion chamber (CVCC) testing platform. In addition, the formation mechanism of the ion current is revealed through CHEMKIN-PRO combustion simulation. The results demonstrate that the peak values and peak timings of the pressure and ion current signals exhibit highly consistent variation patterns as the equivalence ratio changes. Specifically, under lean/stoichiometric combustion, the dominant cations include NH_4^+, NO^+, and H_3O^+, while NH_4^+ predominates under rich combustion. Moreover, the 10% hydrogen-blended condition exhibits similar ion current waveforms and cation concentration variation trends compared with pure ammonia combustion. However, 10% hydrogen blending can significantly enhance the ion current signal intensity, advance the signal peak timing, and promote the chemical ionization of reactants to generate NH_4^+.

Keywords: ammonia; hydrogen; oxygen-enriched combustion; ion current; reaction path

1. Overview

Against the urgent backdrop of global carbon-neutrality, the transition to clean energy for automotive applications has become a critical pillar for achieving low-carbon development goals [1]. Ammonia fuel, due to its carbon-free property, relatively high energy density, and well-established industrial chain foundation, has emerged as a highly promising green alternative [2–4], which has already undergone initial engineering application in marine engines [5]. However, issues such as slow combustion velocity and ignition difficulties severely restrict its direct application in internal combustion engines (ICEs) [6]. In response to this, hydrogen blending and oxygen-enriched combustion are commonly used to improve the combustion performance of ammonia. Blending a small amount of hydrogen can significantly improve ignition stability and accelerate flame propagation [7,8]. Meanwhile, increasing the oxygen concentration can effectively shorten the ignition delay period and enhance combustion intensity, thereby significantly improving the indicated thermal efficiency of the engine and reducing the emissions of unburned NH_3 [9]. The strategy of oxygen enrichment and hydrogen blending can enhance the combustion stability of ammonia, providing a promising pathway for the deep decarbonization of automotive energy.

However, the oxygen-enriched atmosphere and hydrogen blending increase the risk of knock. When the hydrogen blending ratio or oxygen concentration exceeds a critical threshold, the rapidly released heat generates intense pressure waves in the confined space. These pressure waves, after reflection and superposition, can form self-sustaining detonation waves [10,11]. Meanwhile, the extremely low ignition energy of hydrogen makes the unburned mixture more prone to compression ignition. In contrast, the anti-knock property of ammonia competes with the knock-prone characteristic of hydrogen, resulting in a nonlinear threshold feature in knock behavior [12–14], which exacerbates the difficulty of abnormal combustion detection. Therefore, it is urgent to explore appropriate methods for the on-board detection of abnormal combustion in ammonia-hydrogen fuel systems, further providing support for combustion optimization.

A variety of in-cylinder combustion detection techniques have been developed, such as engine block vibration detection, pressure sensor detection, and optical diagnosis. However, the large-scale engineering application of these methods is limited by high costs, short service life, or the need for complex engine modifications [15]. In contrast, ion current detection technology is regarded as one of the most promising real-

Copyright: © 2026 by the authors. This is an open access article under the terms and conditions of the Creative Commons Attribution (CC BY) license (https://creativecommons.org/licenses/by/4.0/).
Publisher's Note: Scilight stays neutral with regard to jurisdictional claims in published maps and institutional affiliations.

time in-cylinder combustion monitoring technologies due to its advantages of low cost, fast response time, and no need to modify the engine structure [16]. For hydrocarbon fuels, the application of ion current detection technology has been extensively studied [17]. The characteristic parameters of the signal, such as amplitude, phase, and frequency, can effectively reflect combustion behavior, enabling diagnosis and feedback control of abnormal combustion [18,19]. However, the flame ionization mechanism of ammonia-hydrogen differs fundamentally from that of hydrocarbon fuels, and research on ion current diagnostics for ammonia-hydrogen remains in its infancy. Cherepanov et al. [20] identified NH_4^+, NO^+, and H_3O^+ as the primary charged species responsible for ion current in ammonia combustion using a Botha-Spalding burner. Under engine-like conditions, Zhou et al. [21] demonstrated that the ion current signals present a similar oscillation frequency compared with the pressure signals under different combustion conditions. Furthermore, it was also found that the type and concentration proportion of dominant cations under different equivalence ratios determine the single/double-peak characteristic of the ion current waveform. However, existing studies have not clearly clarified the key reaction pathways and the evolution mechanism of ion concentration, limiting the application and development of ion current detection technology in ammonia-hydrogen engines.

This study investigates the characteristics of pressure and ion current signals of ammonia oxygen-enriched combustion utilizing a CVCC testing platform. The feasibility of ion-current technology application in ammonia-fueled engines is verified by analyzing the amplitude and phase of the two signals. On this basis, CHEMKIN-PRO simulations are used to analyze the variation in cation concentration and key reaction pathways under different equivalence ratios, which reveals the formation mechanism of the ion current. In addition, hydrogen is blended into the ammonia to investigate the ion current characteristics of ammonia-hydrogen blended combustion. This study is expected to provide experimental foundation and theoretical support for the diagnosis and optimization of ammonia-hydrogen combustion based on ion current detection technology.

2. Experimental and Numerical Setups

2.1. Experimental Setup

Figure 1 shows the schematics of (a) the CVCC testing platform and (b) the ion current detection module established in this study. The CVCC is forged from stainless steel and features a rectangular cavity with dimensions of 300 mm × 50 mm × 50 mm. On the cavity surface, two square glass observation windows with a size of 55 mm × 55 mm are symmetrically arranged. In addition, a spark plug is installed 69 mm away from the left side of the cavity for ion current detection, and a pressure sensor is installed 171 mm away from the same side. The models of experimental equipment for the remaining subsystems are listed in Table 1, including the ignition system, signal acquisition system, data acquisition system, and gas intake-exhaust system.

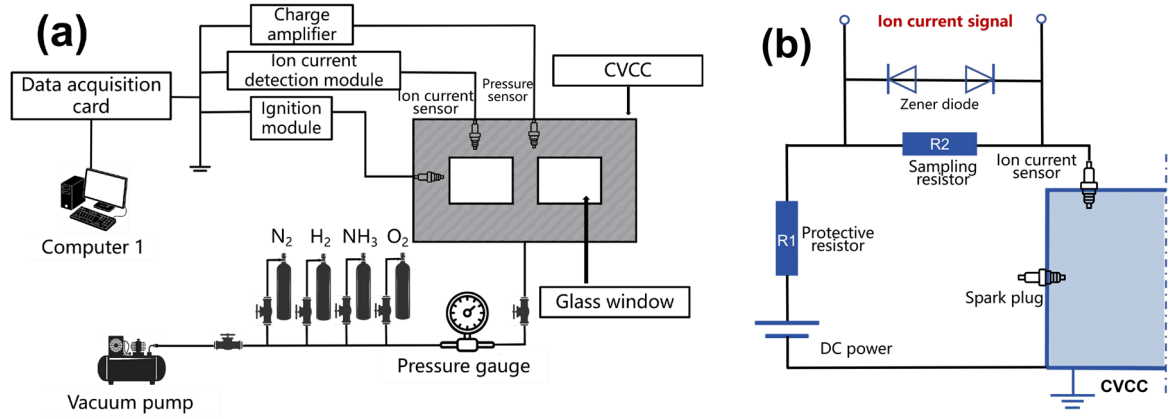


Figure 1. Schematics of (**a**) the CVCC test system and (**b**) the ion current detection module.

Table 1. Models of experimental devices for the CVCC test system.

Experimental Device	Model
Signal trigger	ZK-PP1/PWM
Ignition coil	TFK00405041
Signal amplifier	Kistler 5011B10
Pressure sensor	AVL GH15DK
Pressure gauge	YB-80A
Vacuum pump	2XZ-2 rotary vane type
Signal acquisition card	NI6251

To ensure the accuracy and repeatability of the experimental data, this study designed a standardized procedure for gas mixing, ignition triggering, and signal acquisition. After evacuating the CVCC to a vacuum state, the experimental gases were sequentially introduced into the chamber until the target pressure was reached, followed by a three-minute standing period to ensure no gas flow was observable in the schlieren images. Upon activation, the signal trigger sends pulse signals to synchronously initiate ignition and signal acquisition. Specifically, the data acquisition card recorded the pressure and ion current signals synchronously at a sampling frequency of 50,000 Hz.

Experimental conditions are presented in Table 2. Equivalence ratio (Φ) was varied from 0.6 to 1.2 to cover lean, stoichiometric, and rich combustion conditions. Meanwhile, comparative experiments were conducted using 100% NH_3 and 90% NH_3 + 10% H_2 blend as the fuel. The comparison was designed to reveal the impact of hydrogen addition on cation concentration as well as ion current signals. Specifically, each operating condition was repeated at least three times to avoid deviations in a single experiment that might be caused by operational fluctuations, instrument noise, or environmental interference.

Table 2. Settings of test condition parameters.

Parameter	Value
Signal acquisition frequency (Hz)	50,000
Initial temperature (K)	293
Initial pressure (kPa)	100
Oxidizer mixture (volume fraction)	90% O_2 + 10% N_2
Fuel mixture (volume fraction)	100% NH_3, 90% NH_3 + 10% H_2
Equivalence ratio (Φ)	0.6–1.2, ΔΦ = 0.1

2.2. Numerical Setup

To investigate the combustion mechanism, this study analyzed cation concentration variations under different initial conditions (equivalence ratio and hydrogen blending ratio) and identified the dominant elementary reactions for each combustion condition. Chemical kinetic analysis of ammonia combustion under oxygen-enriched conditions was carried out using CHEMKIN-PRO (ANSYS, Canonsburg, PA, USA), adopting the ammonia-hydrogen combustion mechanism proposed by Cherepanov et al. [20]. The premixed laminar flame burner model was mainly employed to analyze the initial flame propagation behavior, with the simulation conditions listed in Table 3. Considering that the electrical mobility of free electrons in flame plasma is orders of magnitude higher than that of bulky cations, electrons act as the primary charge carriers governing the macroscopic ion current. Consequently, the simulated electron density was selected as the most direct proxy for electrical conductivity [22]. Within the investigated range of equivalence ratios, the simulated electron density matched well with the experimentally measured maximum ion current signal, as shown in Figure 2, which verified that the adopted reaction mechanism can effectively predict the evolution of ion and electron concentrations during ammonia combustion, and provided theoretical support for the waveform analysis of ion current signals.

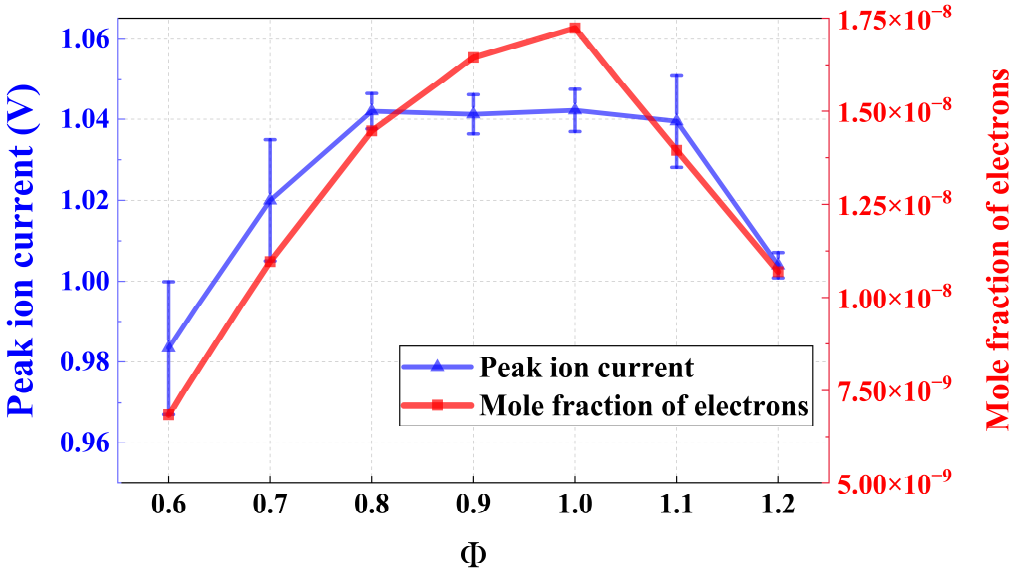


Figure 2. Validation of the simulation.

Table 3. Settings of the numerical simulation.

Parameter	Value
Model	Premixed Laminar Burner
Problem type	Solve Gas Energy Equation
Initial temperature (K)	293
Initial pressure (kPa)	100
Oxidizer mixture (volume fraction)	90% O_2 + 10% N_2
Fuel mixture (volume fraction)	100% NH_3, 90% NH_3 + 10% H_2
Equivalence ratio (Φ)	0.6–1.2, ΔΦ = 0.1

3. Results and Discussion

3.1. Ion Current Characteristics of Ammonia Combustion

Figure 3 presents the pressure and ion current signals of pure-ammonia oxygen-enriched combustion. Previous studies have demonstrated that the characteristic oscillation frequencies of ammonia combustion are approximately 2000 Hz, 4000 Hz, and 6000 Hz. Therefore, a low-pass filter with a cutoff frequency of 1500 Hz is applied to ensure that the smoothed curves can clearly reflect the general trend of signal variations. The processed figures keep the raw signals in light color to clearly show the experimental results. It is worth noting that the pressure signals show an abnormal drop at approximately 5 ms under all conditions. This fluctuation is caused by a local low-pressure vortex formed as the flame front passes through the pressure sensor cavity, and it does not affect the overall analysis of pressure signals. It can be seen that the overall waveform of pressure and ion current signals exhibits high similarity under different equivalence ratios. The ion current signal remains at the baseline level during the initial ignition stage. As the flame propagates to the ion current sensor, charged species such as cations and electrons produced by chemical ionization in the flame migrate directionally under the bias voltage applied to the measuring electrodes. Consequently, the ion current rises instantaneously and forms a distinct chemical ionization peak, followed by a short plateau. Subsequently, as the pressure signal approaches its peak, the mixture is fully combusted and releases a large amount of heat. After this point, the temperature gradually decreases, leading to a decline in both pressure and ion current signals.

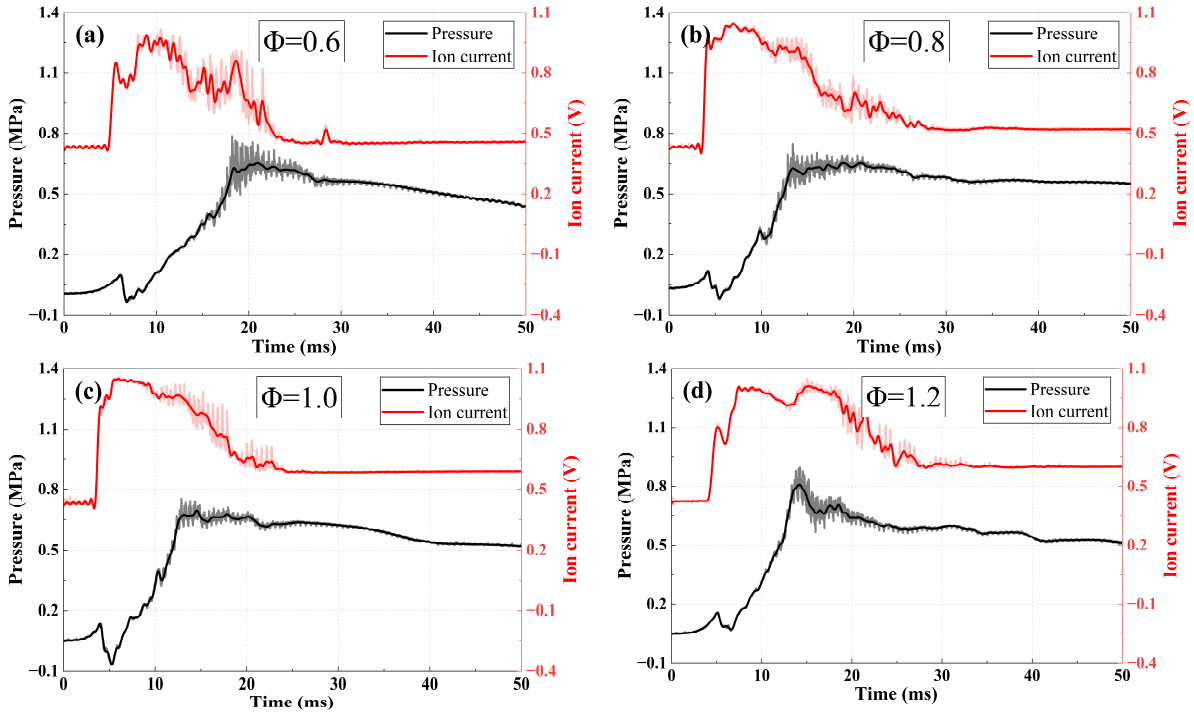


Figure 3. Pressure and ion current signals (**a**) Φ = 0.6; (**b**) Φ = 0.8; (**c**) Φ = 1.0; (**d**) Φ = 1.2.

Based on Figure 3, the peak values and the time at which the signals reach the peaks (defined as peak timings) of the pressure and ion current signals are extracted from the processed curves, as presented in Figure 4. Notably, range error bars are included in Figure 4 to indicate the maximum, minimum, and average values obtained from three repeated tests. The peak values of both pressure and ion current signals show a similar variation trend. Specifically, the peak values increase initially and then decline as the equivalence ratio increases, with the maxima

occurring under near-stoichiometric combustion. Similarly, the peak timings advance first and then delay as the equivalence ratio increases. These phenomena can be explained by the fact that near-stoichiometric combustion provides a stoichiometric mixture of fuel and oxidizer, yielding the most intense combustion and the highest reaction temperature. Consequently, a higher heat release rate produces the maximum pressure peak. Meanwhile, the high-temperature atmosphere significantly promotes the chemical ionization of species and the generation of charged particles, which enhances the intensity of the ion current signal.

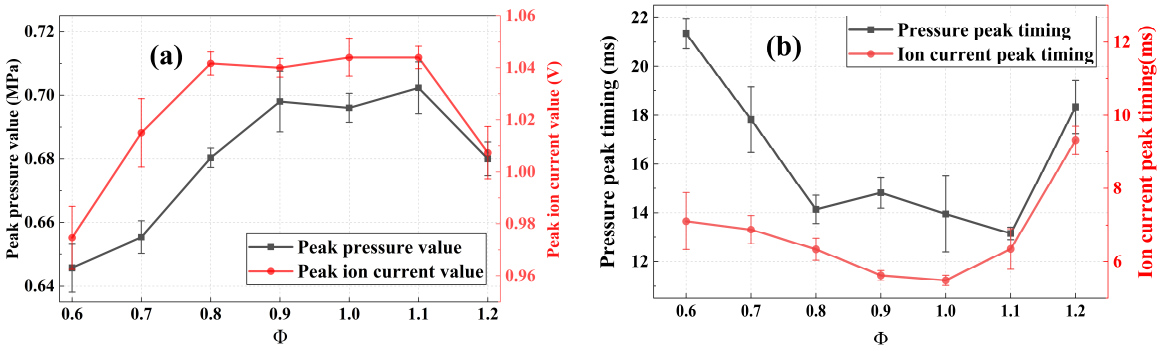


Figure 4. (**a**) Peak values and (**b**) peak timings of pressure and ion current signals.

The above results demonstrate that the ion current signal during oxygen-enriched ammonia combustion correlates strongly with the equivalence ratio. Additionally, the ion current can effectively characterize the combustion behavior inside the CVCC, which validates the feasibility of ion current detection technology for combustion diagnosis and optimization.

3.2. Analysis of Cation Reaction Kinetics in Oxygen-Enriched Ammonia Combustion

Essentially, an ion current arises from the directional migration of electrons in a flame under an external electric field. The mobility of cations is much lower than that of electrons under low voltage conditions. However, the high mobility of electrons is restricted by the electrostatic force of cations, leading to a uniform spatial distribution of the two species [22]. Therefore, the analysis of the cation concentration during ammonia combustion can directly reflect the core characteristics of the ion current, providing a key basis for interpreting ammonia combustion behavior.

During the combustion of pure ammonia or ammonia/hydrogen blends, the dominant cations include NH_4^+, NO^+, as well as H_3O^+, and seven key elementary reactions are involved, as listed in Table 4. Although the adopted mechanism may underestimate the relative abundance of NO^+ under fuel-lean conditions, as noted in the original kinetic study [20]. The model is expected to capture the variation trends of the dominant cations and the total cation concentration, providing a reliable foundation for the qualitative analysis of the ion current signals. Therefore, this study employs CHEMKIN-PRO to conduct a chemical kinetic analysis of pure ammonia combustion across various equivalence ratios. By identifying the dominant pathways for cation formation and consumption, the underlying mechanisms governing the formation and evolution of the ion current signal can be comprehensively clarified.

Table 4. Key reactions involving N-atom-bearing cations are included in the ion chemistry mechanism [20].

Number	Chemical Reaction Equation	Role
R[1]	$NH_4^+ + e^- \Leftrightarrow 2H + NH_2$	Chemical ionization/recombination
R[2]	$NH_4^+ + e^- \Leftrightarrow H_2 + NH_2$	Chemical ionization/recombination
R[3]	$NH_4^+ + e^- \Leftrightarrow H + NH_3$	Chemical ionization/recombination
R[4]	$H_3O^+ + NH_3 \Leftrightarrow H_2O + NH_4^+$	Proton transfer
R[5]	$NO^+ + e^- \Leftrightarrow N + O$	Chemical ionization/recombination
R[6]	$NO + H_3O^+ \Leftrightarrow NO^+ + H_2O + H$	Proton transfer

Figure 5 shows the concentration evolutions of the cations NH_4^+, NO^+, and H_3O^+, as well as the total concentration of these three cations. Specifically, the fuel is 100% NH_3, and the oxidizer is 90% O_2 + 10% N_2 under the initial condition of 293 K and 100 kPa. The curves at each equivalence ratio in the figure are divided into three stages according to the variation trends of the cations, where yellow, green, and blue respectively correspond to the first, second, and third stages. It can be seen from the figure that under lean-burn and

stoichiometric conditions, the dominant cations are NH_4^+, NO^+, and H_3O^+, and the variation trends of cation concentration are similar at different equivalence ratios. In contrast, the dominant cation under rich-burn conditions includes only NH_4^+. In Figure 5d, the total cation concentration curve visually overlaps with the $NH4^+$ curve. It can be attributed to the reason that $NH4^+$ constitutes nearly the entirety of the total cations under rich combustion conditions. Therefore, to reveal the mechanisms behind the two distinct ion- dominated patterns, namely the multi-cation dominance under lean/stoichiometric combustion and the single-cation dominance under rich combustion, this study performs a chemical kinetic analysis for typical operating conditions of the two patterns. In particular, combustion at $\Phi = 0.6$ and $\Phi = 1.2$ is chosen as the research cases.

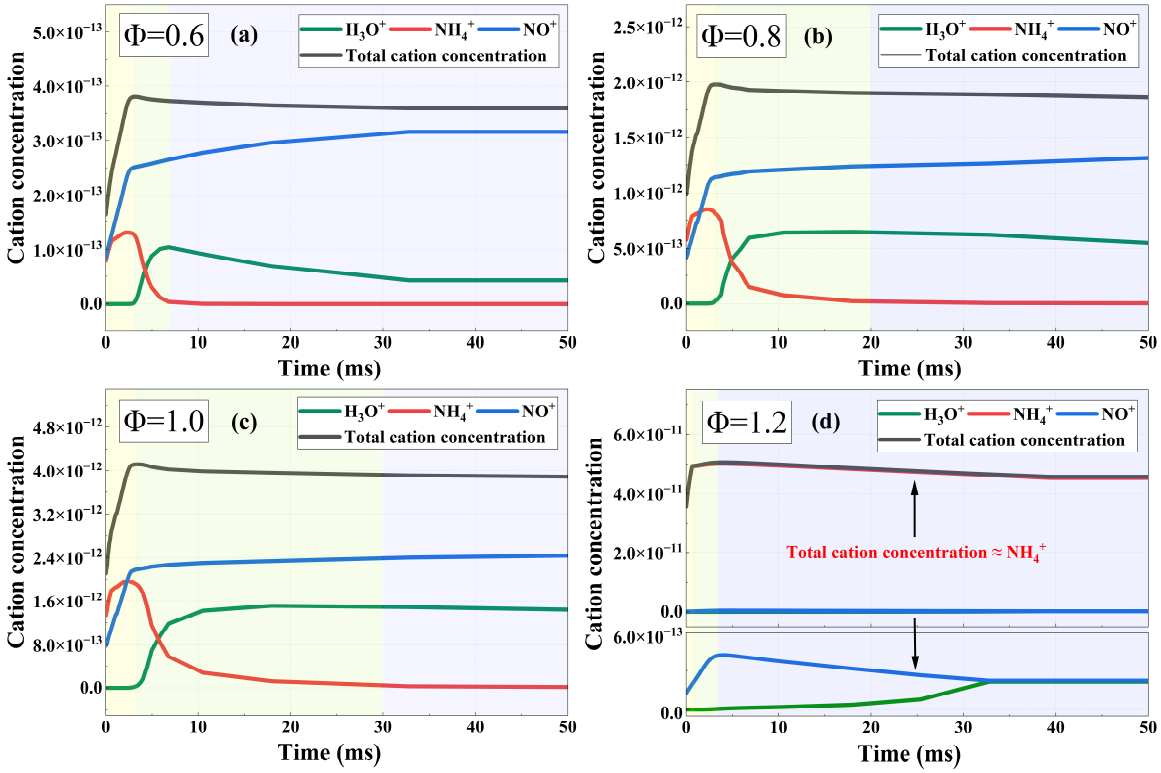


Figure 5. Cation concentration of pure ammonia combustion at (**a**) $\Phi = 0.6$; (**b**) $\Phi = 0.8$; (**c**) $\Phi = 1.0$; (**d**) $\Phi = 1.2$.

Figure 6 shows the rate profiles of the dominant elementary reactions in the first two stages at $\Phi = 0.6$. Specifically, the absolute reaction rates for the formation and consumption of the three cations are presented for sensitivity analysis, which enables the identification of the dominant reaction pathways. The first stage corresponds to the early combustion period, when the concentrations of reactants and radicals are relatively high, leading to intense chemical ionization. Most NH_3 is oxidized by OH to produce N atoms, which further participate in chemical ionization via reaction R[5] $N + O \Leftrightarrow NO^+ + e^-$ to generate NO^+. Meanwhile, NH_2 produced by the oxidation of a small fraction of NH_3 is converted into NH_4^+ through reaction R[1] $2H + NH_2 \Leftrightarrow NH_4^+ + e^-$. The rapid accumulation of NO^+ and NH_4^+ produced by chemical ionization gives rise to a sharp increase in the ion current signal. In this stage, the total cation concentration curve gradually forms a peak, which is consistent with the chemical ionization peak of ion current signals in Figure 3. In addition, the proton-transfer reaction R[6] $NO^+ + H_2O + H \Leftrightarrow NO + H_3O^+$ consumes a small amount of NO^+ to produce H_3O^+, which is further converted into NH_4^+ via R[4] $H_3O^+ + NH_3 \Leftrightarrow H_2O + NH_4^+$. The two reactions proceed at similar rates, so H_3O^+ can be regarded as a proton transfer bridge between NO^+ and NH_4^+ in this stage, with its concentration maintained at an extremely low level.

In the second stage, reactants and radicals are substantially consumed, making it difficult to sustain the chemical ionization reactions, which rely on the participation of radicals. As a result, the increase in NO^+ concentration gradually slows down. In addition, as the reactant NH_3 is nearly depleted and the concentration of H_2O increases, the equilibrium of reaction R[4] $H_3O^+ + NH_3 \Leftrightarrow H_2O + NH_4^+$ shifts toward the reverse direction, leading to a rapid rise in H_3O^+ concentration. Although a small amount of NH_4^+ is produced by minor side reactions during this process, the NH_4^+ concentration still decreases rapidly to an extremely low level. Generally, the total cation concentration in this stage shows a slowly decreasing trend, which corresponds to the plateau region of the ion current curves in Figure 3.

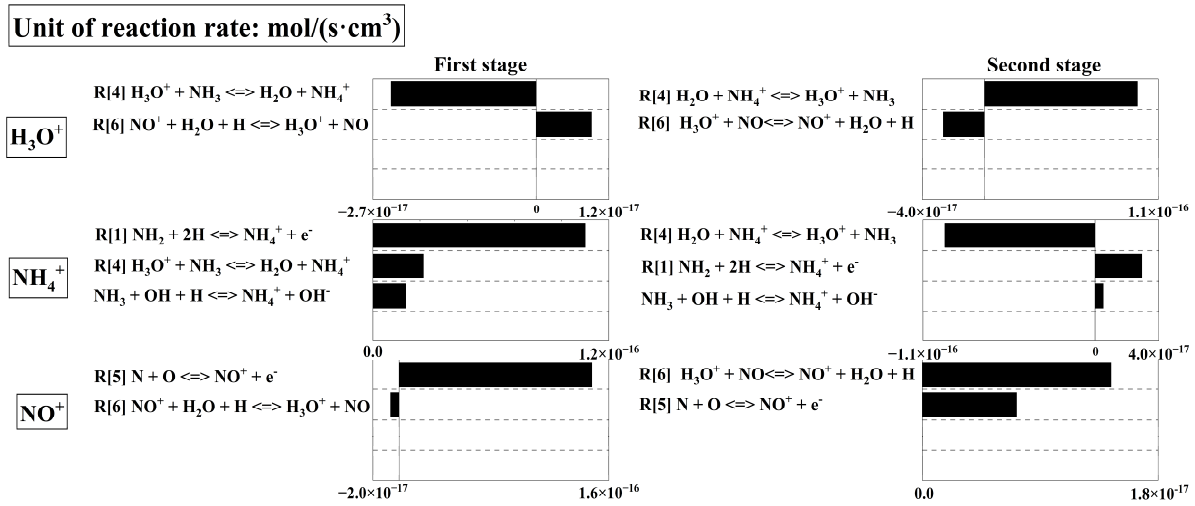


Figure 6. Sensitivity analysis of formation and consumption reactions of NH_4^+, NO^+, and H_3O^+ at $\Phi = 0.6$.

Based on the above analysis, the dominant reaction pathways of the three main cations can be obtained, as shown in Figure 7. Under lean-burn and stoichiometric combustion conditions, the dominant cations include NH_4^+, NO^+, and H_3O^+. In the early stage of combustion, the main cations contributing to the ion current are NH_4^+ and NO^+, both of which originate from chemical ionization reactions. However, in the middle and late stages of combustion, NO^+ and H_3O^+ become the dominant cations determining the ion current intensity. In this stage, R[4] plays a dominant role in this stage, accompanied by substantial consumption of NH_4^+ and production of H_3O^+. In addition, the waveform of the ion current corresponds well to the variation trend of cation concentration.

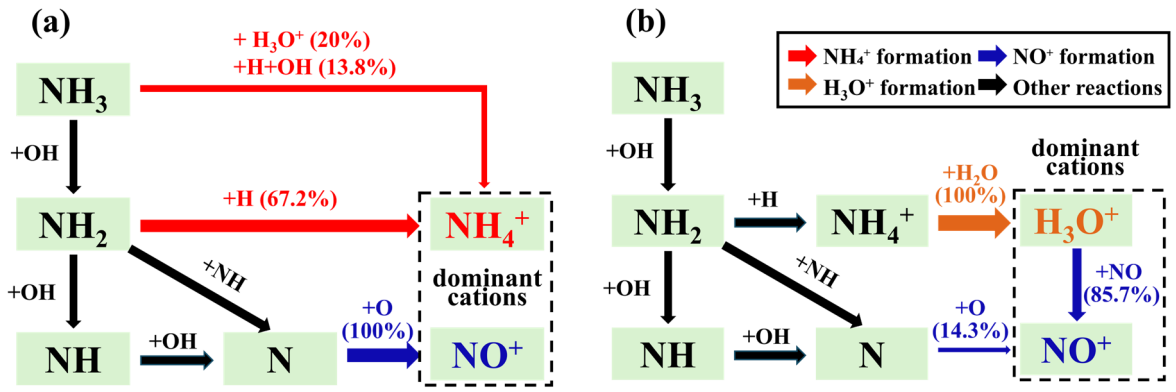


Figure 7. Dominant reaction pathways of oxygen-enriched ammonia combustion during (**a**) the first stage and (**b**) the second stage at $\Phi = 0.6$.

Compared with the lean-burn and stoichiometric combustion, the dominant cation under rich-burn combustion is solely NH_4^+, whose concentration remains at a high level of 10^{-11} throughout the process. In contrast, the concentrations of H_3O^+ as well as NO^+ only fluctuate on the order of 10^{-13}. Similarly, this study divides the combustion into three stages, and the formation/consumption rates of the main cations under these conditions are shown in Figure 8.

In the first stage, the NH_4^+ concentration rises extremely rapidly to a peak at the early stage of combustion, which arises from chemical ionization reactions, namely reaction R[1]–R[3]. Meanwhile, NO^+ is also produced by the corresponding chemical ionization reaction R[5], which is consistent with the trend observed under lean-burn and stoichiometric combustion conditions. However, the reaction rate of R[1] is two orders of magnitude higher than that of R[5]. This can be attributed to the lower oxygen concentration under rich-burn conditions compared with lean-burn and stoichiometric combustion conditions. From the reaction pathways shown in Figure 7, the formation of N atoms required for R[5] highly depends on the oxidation of NH_3 by OH radicals. The production of OH radicals relies on the reaction $H + O_2 \Leftrightarrow O + OH$. Therefore, the poor-oxygen atmosphere under rich-burn conditions restricts the formation of N atoms, resulting in a consistently low concentration of NO^+. This explains why NH_4^+ is the only dominant cation under rich-burn combustion.

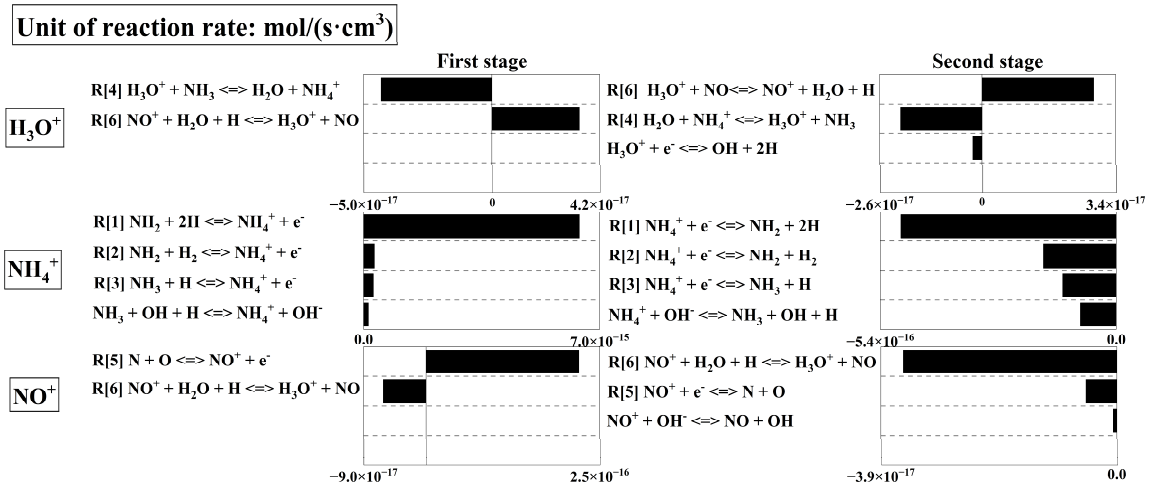


Figure 8. Sensitivity analysis of formation and consumption reactions of NH_4^+, NO^+, and H_3O^+ at Φ = 1.2.

After the first stage, the concentration of the dominant cation NH_4^+ shows a slow and steady downward trend from its earlier high peak, remaining generally on the order of 10^{-11}. This can be attributed to the reversal of Reactions R[1]–R[3], corresponding to chemical recombination. However, the rate of chemical recombination at this stage is only about 1/10 that of the chemical ionization reactions in the first stage. Subsequently, the reactions approach equilibrium. Based on the above analysis, the dominant formation pathways of cations under rich-burn combustion are illustrated in Figure 9. Given that NH_4^+ is absolutely dominant while the concentrations of NO^+ and H_3O^+ are extremely low, only the dominant formation pathway of NH_4^+ is presented here.

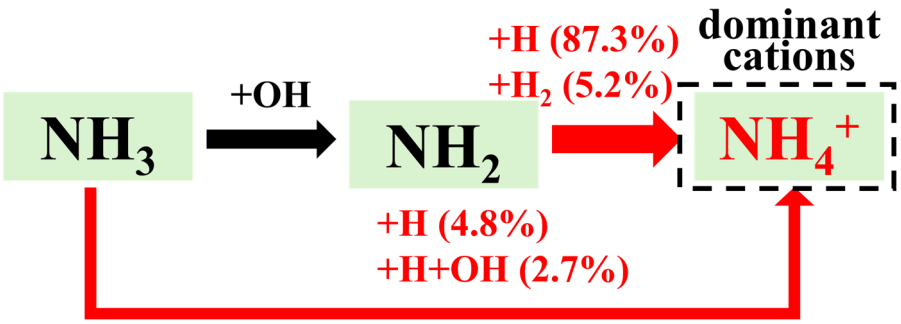


Figure 9. Dominant reaction pathways of oxygen-enriched ammonia combustion at Φ = 1.2.

3.3. Impact of Hydrogen Blending on Ion Current in Ammonia Combustion

To investigate the effect of hydrogen addition on oxygen-enriched ammonia combustion, the 10% hydrogen-blended ammonia combustion is investigated and compared with pure ammonia combustion. Figure 10 shows the ion current signals of two fuels under four equivalence ratios. Overall, the two signals exhibit similar waveform characteristics. In addition, it can be observed that the ion current intensity of ammonia-hydrogen blended combustion is significantly higher than that of pure ammonia throughout the entire combustion. Figure 11 presents (a) the peak values and (b) peak timings at various equivalence ratios. Similarly, it can be seen that, for both fuel systems, the peak signal intensity first increases and then decreases, while the time to peak occurs earlier and then later as the equivalence ratio increases from 0.6 to 1.2. This trend is consistent with that observed in the above analysis in pure ammonia combustion. Compared with pure ammonia combustion, the 10% hydrogen-blended combustion exhibits a higher peak value and a shorter time to reach the peak under all equivalence ratios. This can be attributed to the higher chemical reactivity and faster burning velocity of hydrogen. As a result, the addition of hydrogen significantly accelerates the overall combustion reaction rate, thereby greatly increasing the formation rate of charged particles.

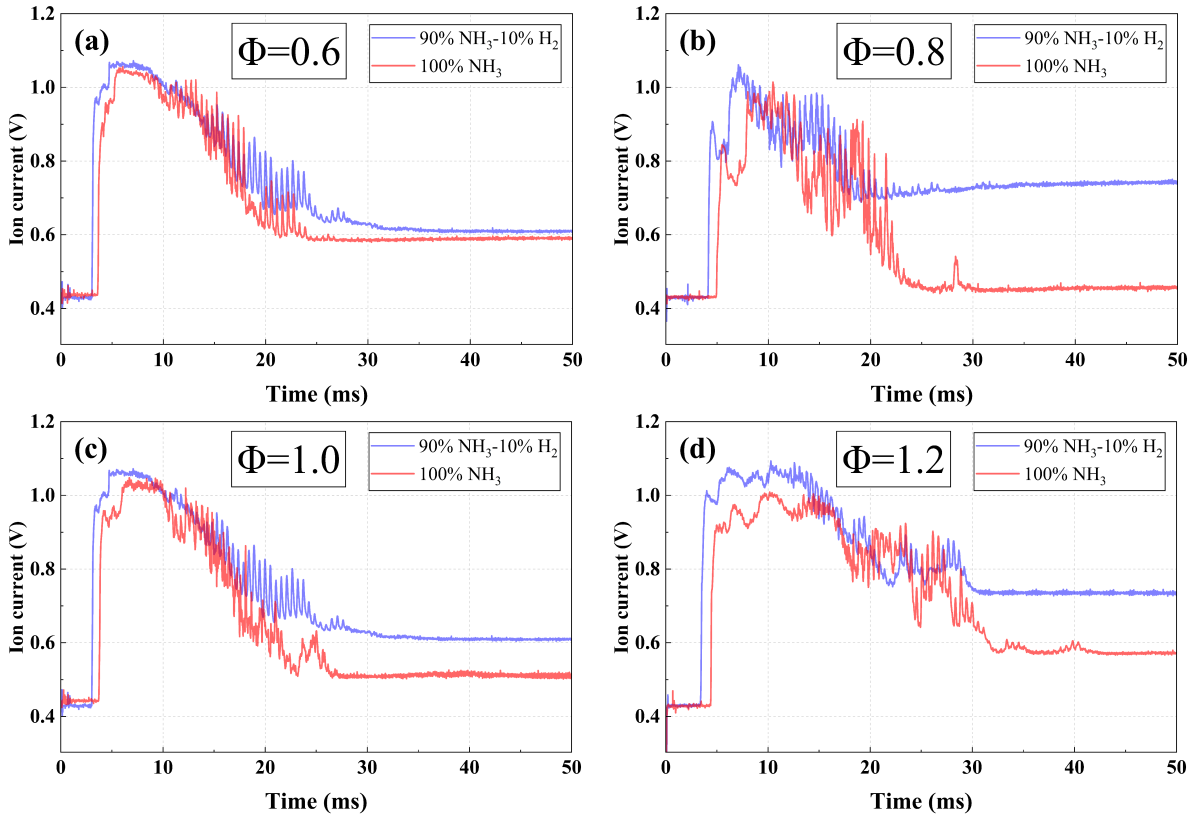


Figure 10. Comparison of ion current signals before and after hydrogen blending at (**a**) Φ = 0.6; (**b**) Φ = 0.8; (**c**) Φ = 1.0; (**d**) Φ = 1.2.

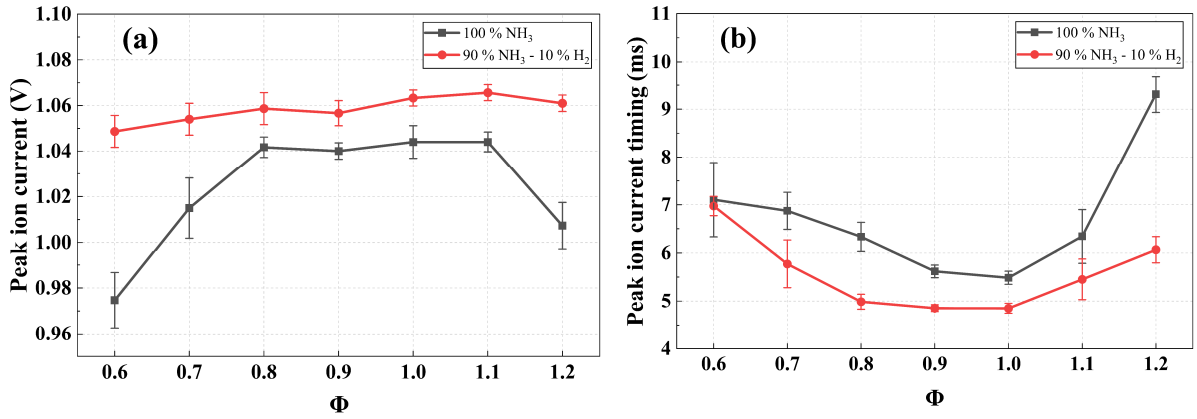


Figure 11. The (**a**) peak values and (**b**) peak timings of the ion currents before and after hydrogen blending.

To clarify this phenomenon, a kinetic analysis of ammonia-hydrogen blended combustion is performed in this study. Figure 12 presents the cation concentration during the 10% hydrogen-blended combustion at different equivalence ratios. It can be seen that NH_4^+, NO^+, and H_3O^+ are the dominant cations under lean-burn and stoichiometric conditions, while only NH_4^+ dominates under rich-burn conditions. This trend is identical to that of pure ammonia combustion, and the concentration evolution of the three main cations at different combustion stages also shows similar behavior. From the viewpoint of cation concentration variation, the similar ion current waveforms between pure ammonia and ammonia-hydrogen blended combustion can be well explained. Essentially, ammonia is an effective hydrogen carrier and can decompose to produce a small amount of hydrogen during combustion. Therefore, the overall waveform characteristics of the ion current and the fundamental mechanisms governing the waveform variation in ammonia-hydrogen blended combustion are basically consistent with those in pure ammonia combustion.

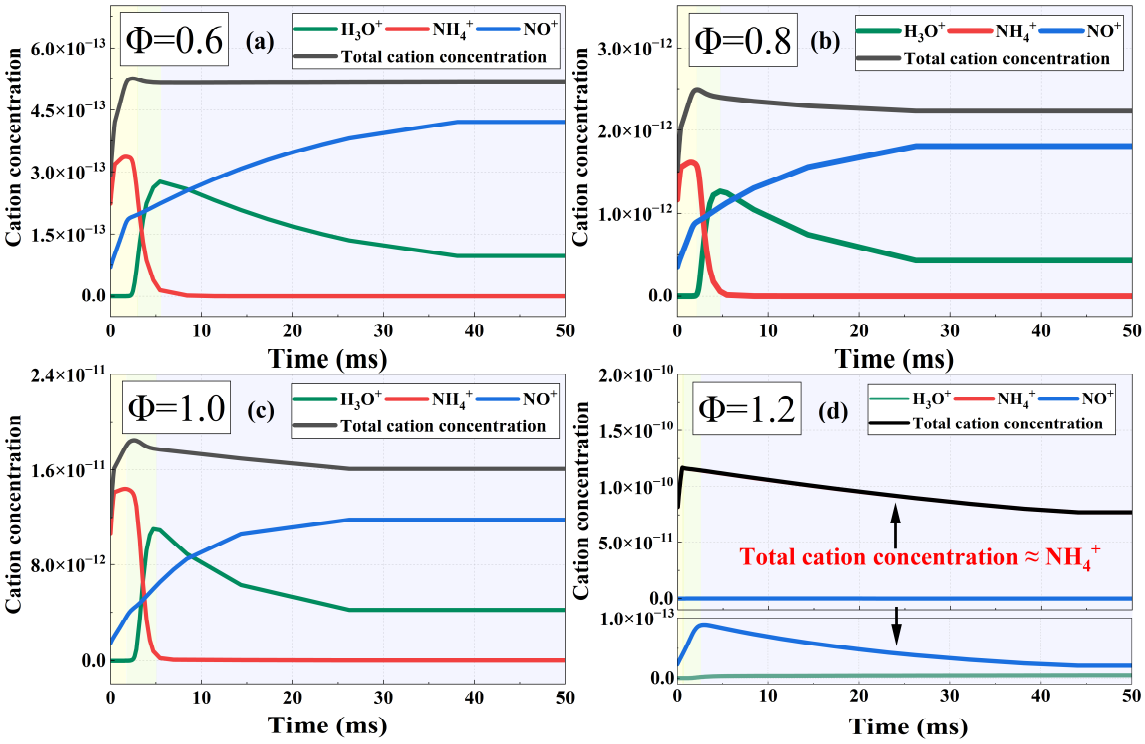


Figure 12. Cation concentration of 10% hydrogen-blended combustion at (**a**) Φ = 0.6; (**b**) Φ = 0.8; (**c**) Φ = 1.0; (**d**) Φ = 1.2.

The 10% hydrogen-blended case presents a higher cation concentration throughout the combustion. Compared with pure ammonia, the concentration of the dominant cation during blended combustion is increased by 1–2 orders of magnitude overall, accompanied by a faster growth rate and a higher peak value. This remarkable increase in cation concentration directly matches the experimental observation that the ion current signal intensity of hydrogen-blended fuel is higher than that of pure ammonia combustion. Thus, it is confirmed that hydrogen blending has a significant promoting effect on the ion formation reactions.

Furthermore, under the condition of 10% hydrogen-blended, the relative concentration proportion of NH_4^+ at the early combustion stage is significantly higher than pure ammonia combustion under lean-burn and stoichiometric combustion. To quantify this phenomenon, this study defines the ratio of the NH_4^+ concentration peak to the total concentration of all cations as the NH_4^+ peak proportion coefficient $R_{NH_4^+}$, as shown in Equation (1):

$$R_{NH_4^+} = \frac{c_{NH_4^+,peak}}{c_{NH_4^+,peak} + c_{NO^+} + c_{H_3O^+}} \quad (1)$$

where $c_{NH_4^+,peak}$ represents the peak concentration of NH_4^+, while c_{NO^+} and $c_{H_3O^+}$ represent the concentrations of NO^+ and H_3O^+ at the same moment, respectively.

Figure 13 shows the $R_{NH_4^+}$ under lean and stoichiometric combustion conditions. It can be clearly observed that the proportion of NH_4^+ at its peak moment in the 10% hydrogen-blending combustion is higher than that in pure ammonia combustion. This study selects the operating point at Φ = 1.0 and 2.5 ms for analysis, because the concentration proportion of NH_4^+ is the highest at this condition, which yields the most obvious analytical results. Figure 14 presents the formation and consumption reaction rates of H_2. It is found that H atoms are involved in the products of several major H_2-consuming reactions, which proceed at high rates, leading to a high H-atom concentration in the early reaction stage. Consequently, reaction R[1], namely $2H + NH_2 \Leftrightarrow NH_4^+ + e^-$, tends to proceed toward the direction of chemical ionization. In addition, the chemical ionization process for NH_4^+ formation is endothermic, and the higher reactivity and faster burning velocity of hydrogen raise the overall temperature, which in turn further promotes the generation of NH_4^+. Consequently, the ion concentration proportion of NH_4^+ in the ammonia–hydrogen blended combustion is significantly higher than that in pure ammonia combustion.

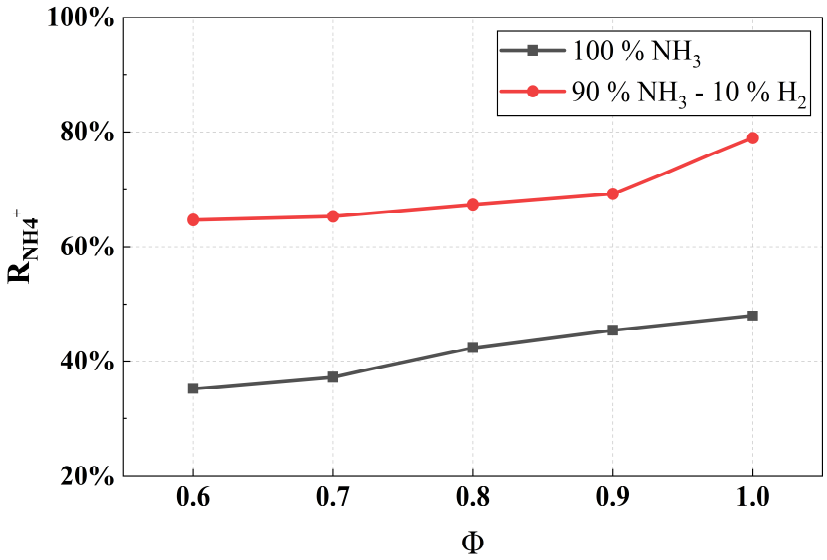


Figure 13. Concentration proportion of NH_4^+ at the peak moment.

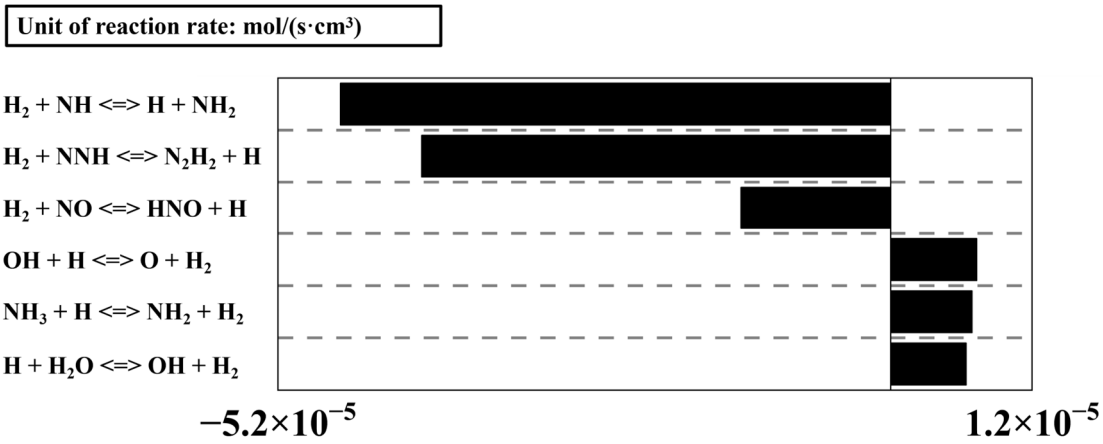


Figure 14. Sensitivity analysis of H_2 consumption and formation reactions under 10% hydrogen-blending condition.

4. Conclusions

In this study, experiments were conducted based on a CVCC testing platform to investigate the waveform characteristics of ion current signals during pure ammonia and ammonia–hydrogen blended combustion under oxygen-enriched conditions. Additionally, chemical kinetic analysis was performed using CHEMKIN-PRO to clarify the formation mechanism and influencing factors of the ion current signal, as well as its dominant reaction pathways at various equivalence ratios. Moreover, the effects of hydrogen addition on the ion current and cation concentration in ammonia combustion were further explored. The main conclusions are drawn as follows:

(1) Under oxygen-enriched conditions, the peak values and peak timings of the ion current and pressure signals during pure ammonia combustion exhibit highly consistent variations as the equivalence ratio increases. Meanwhile, the evolution of the total cation concentration is in good agreement with the ion current waveform. Near stoichiometric combustion, both signals reach the maximum peak values and the earliest peak timings. As the mixture becomes either leaner or richer, the peak values decrease, and the peak timings are delayed.

(2) Under lean-burn and stoichiometric combustion conditions, the dominant cations are NH_4^+, H_3O^+, and NO^+, while only NH_4^+ is dominant under rich-burn conditions. NH_4^+ is mainly produced via chemical ionization reactions in the early combustion stage, with the dominant reaction pathway being $NH_3 \rightarrow NH_2 \rightarrow NH_4^+$. H_3O^+ exhibits an extremely low concentration at the early stage, and is mainly formed through proton transfer reactions with NH_4^+, following the dominant pathway $NH_3 \rightarrow NH_2 \rightarrow NH_4^+ \rightarrow H_3O^+$. NO^+ is primarily generated by the initial chemical ionization process throughout combustion, with the dominant pathway being $NH_3/O_2 \rightarrow N/O \rightarrow NO^+$. The concentration of NO^+ under rich-burn conditions drops to an extremely low level due to the oxygen-deficient atmosphere.

(3) 10% hydrogen blending can significantly enhance the ion current signal intensity and cation formation rate during ammonia combustion, and promote the chemical ionization generation of NH_4^+. Fundamental waveform characteristics, as well as the underlying mechanisms' behavior under 10% hydrogen blending conditions, remain consistent with pure ammonia combustion. However, the ion current signal exhibits a higher peak value and an earlier peak timing, and the concentration of each cation is increased by 1–2 orders of magnitude overall.

Author Contributions: J.X.: writing—review & editing, writing—original draft, visualization, formal analysis, data curation. G.D: writing—review & editing, project administration, methodology, funding acquisition, conceptualization. Y.Z.: software, investigation, formal analysis, data curation. X.L.: visualization, validation, investigation, data curation. L.L.: writing—review & editing, supervision, project administration, methodology, funding acquisition. All authors have read and agreed to the published version of the manuscript.

Funding: This research was funded by the National Natural Science Foundation of China, No. 52176126, and supported by the Shanghai Key Lab of Vehicle Aerodynamics and Vehicle Thermal Management Systems.

Institutional Review Board Statement: Not applicable.

Informed Consent Statement: Not applicable.

Data Availability Statement: The original contributions presented in this study are included in the article. Further inquiries can be directed to the corresponding authors.

Conflicts of Interest: The authors declare no conflict of interest.

Use of AI and AI-Assisted Technologies: No AI tools were utilized for this paper.

References

1. Wang, G.; Chen, C.; Beshiwork, B.A.; Lin, B. Developing a low-carbon hybrid of ammonia fuel cell and internal combustion engine for carbon neutrality. *Appl. Energy Combust. Sci.* **2023**, *16*, 100214.
2. Zhu, D.; Shu, B. Recent progress on combustion characteristics of ammonia-based fuel blends and their potential in internal combustion engines. *Int. J. Automot. Manuf. Mater.* **2023**, *2*, 1.
3. Pugazhendhi, A.; Bharathi, D.; Aljohani, B.S.; Aljohani, K.; Kamarudin, S.K.; Sekar, M.; Shanmuganathan, R. Sustainable ammonia production, storage, and transport technologies for clean energy applications. *Int. J. Hydrogen Energy* **2025**, *194*, 152504.
4. Liu, Z. Alternative fuels in automotive vehicles. *Int. J. Automot. Manuf. Mater.* **2023**, *2*, 7.
5. Wang, H.; Zhou, P.; Jeong, B.; Mesbahi, A.; Mujeeb-Ahmed, M.P.; Jang, H.; Giannakis, A.; Sykaras, K.; Papadakis, A. Life cycle analysis of ammonia fuelled ship-case ship studies for marine vessels. *J. Clean. Prod*. **2025**, *520*, 146105.
6. Tutak, W.; Jamrozik, A.; Grab-Rogaliński, K.; Pyrc, M.; Gruca, M. Effect of ammonia-hydrogen fuel ratio on combustion stability, performance and emissions of an industrial diesel engine. *Int. J. Hydrogen Energy* **2026**, *205*, 153373.
7. Guo, W.Y.; Liu, G.F.; Hu, T.T.; Shi, M.S.; Su, W.H.; Wu, B.Y. Combustion and emissions of ammonia-hydrogen dual-fuel engine under oxygen-enriched conditions. *Int. J. Hydrogen Energy* **2026**, *211*, 153681.
8. Lu, C.; Chen, W.; Zuo, Q.; Zhu, G.; Zhang, Y.; Liu, Z. Review of combustion performance improvement and nitrogen-containing pollutant control in the pure hydrogen internal combustion engine. *Int. J. Automot. Manuf. Mater.* **2022**, *1*, 7.
9. Tian, J.; Wang, L.; Xiong, Y.; Wang, Y.; Yin, W.; Tian, G.H.; Wang, Z.Y.; Cheng, Y.; Ji, S.B. Enhancing combustion efficiency and reducing nitrogen oxide emissions from ammonia combustion: A comprehensive review. *Proc. Saf. Environ. Prot.* **2024**, *183*, 514–543.
10. Li, H.L.; Ghazi, A.K. Knock in spark ignition hydrogen engines. *Int. J. Hydrogen Energy* **2004**, *29*, 859–865.
11. Purayil, S.T.P.; Al-Omari, S.; Elnajjar, E. Comparative analysis of knock intensity in spark ignition engines using gasoline and hydrogen-gasoline blends. *Int. J. Thermofluids* **2025**, *28*, 101309.
12. Zhang, D.; Wang, Y.; Xie, M.Y.; Cheng, X.P.; Mu, X.Y.; Qiu, Y.B. Optimizing hydrogen injection parameters for enhanced combustion in hydrogen-methane rotary engines. *Int. J. Hydrogen Energy* **2026**, *214*, 153813.
13. Meng, X.L.; Xie, F.X.; Liu, Y.; Yu, Z.B.; Jiang, Y.F.; Wang, Z.Y.; Wang, X.Y.; Jin, Z.H. Effects of ammonia addition and variable valve timing on knocking and performance of ethanol pre-chamber engine with high compression ratio. *Energy* **2025**, *327*, 136342.
14. Zhu, G.; Wang, Y.; Chen, W.; Zuo, Q.; Kou, C.; Ning, D.; Wang, H.; Zhao, M.; Chen, Y. Performance analysis of a spark ignition hydrogen/ammonia dual fuel engine. *Int. J. Automot. Manuf. Mater.* **2025**, *4*, 7.
15. Kwong, M.C.; Kyung, W.K. *Measurement and Analysis of Knock in a SI Engine Using the Cylinder Pressure and Block Vibration Signals*; SAE International: Warrendale, PA, USA, 1994; pp. 56–62.
16. Song, Z.F.; Zhang, X.; Zhang, B.Y. Study on the correlation between ion current integral signal and combustion pressure. *Int. J. Hydrogen Energy* **2022**, *47*, 8060–8070.
17. Li, Y.X.; Gao, Z.Q.; Wu, H.X.; Feng, P.C.; Li, Y.T.; Tan, Y.H.; Du, F.P.; Bi, P. Exploration of the ion current method universality and online combustion monitoring. *Fuel* **2022**, *329*, 125366.
18. Liu, Y.; Deng, J.; Hu, Z.; Li, L. In-cycle combustion feedback control for abnormal combustion based on digital ion

current signal. *Int. J. Engine Res.* **2018**, *19*, 241–249.
19. Dong, G.; Tian, J.; Li, L.; Wu, Z.; Ni, X. Study on the ion current forming process under engine knocking conditions. *Combust. Flame.* **2022**, *241*, 112069.
20. Cherepanov, A.V.; Kiselev, V.G.; Dmitriev, A.M.; Osipova, K.N.; Shmakov, A.G.; Knyazkov, D.A. Ion chemistry in ammonia-hydrogen-oxygen flames. *Proc. Combust. Inst.* **2024**, *40*, 105584.
21. Zhou, Y.; Dong, G.; Miao, X.; Xu, J.; Li, X.; Huang, Y.; Li, L. Ion current characteristics analysis for ammonia-hydrogen combustion diagnostic under oxygen-enriched conditions. *Int. J. Hydrogen Energy* **2025**, *188*, 152067.
22. Dong, G.; Lu, H.; Wu, Z.; Dibble, R.; Li, L. Effect of electric fields on the ion current signals in a constant volume combustion chamber. *Proc. Combust. Inst.* **2019**, *37*, 4865–4872.